CURVATURE-BASED SEGMENTATION OF POWDER BED POINT CLOUDS FOR IN-PROCESS MONITORING

Andrew Chung Chee Law*, Nicholas Southon†, Nicola Senin†,°, Petros Stavroulakis†, Richard Leach†, Ruth Goodridge† and Zhenyu Kong*

*Grado Department of Industrial and Systems Engineering, Virginia Polytechnic Institute and State University, Blacksburg, VA 24060, USA
†Manufacturing Metrology Team, Faculty of Engineering, University of Nottingham, NG8 1BB, UK
°Department of Engineering, University of Perugia, PG 06125, Italy

Abstract

This paper presents a curvature-based analysis of point clouds collected in-process with fringe projection in a polymer powder bed fusion process. The three-dimensional point clouds were obtained from outside of the build chamber with a fringe projection measurement system which was provided with access through an observation window. The curvature-based thresholding of powder bed point clouds demonstrates the ability to separate consolidated areas from the powder bed effectively. This segmentation of the point clouds with masks enables the detection of changes in the outline of consolidated areas between layers, computation of average drop due to the consolidation of the powder bed and separate analysis of both powder bed and consolidated areas. The high-level insights extracted from the analysis of the point clouds could improve process control strategies, such as in-line defect detection during an additive manufacturing build as well as an in-process feedback system for tuning the optimal values of additive process parameters. In summary, we show curvature-based thresholding as an effective segmentation for fringe projection point clouds, which can be further applied to detect defects, such as geometric defects and dimensional inaccuracy.

Keywords: Additive Manufacturing, Polymer Powder Bed Fusion, In-Process Monitoring, Fringe Projection, 3D Point Cloud Processing, Curvature, Segmentation

Corresponding author: aclaw@vt.edu

1. Introduction

Additive manufacturing (AM) has the potential to produce complex, functional components in small runs at unit costs competitive or better than other forms of manufacturing. To utilize these potential benefits, however, more research and development is essential in all aspects of production, ranging from a part material properties to its dimensional accuracy [1] and surface topography [2]. The specific AM process studied in this paper is polymer laser powder bed fusion (LPBF), which utilizes a laser beam as a thermal energy source to selectively fuse the areas of a polymer powder

bed. The bed is then lowered, and more powder is spread to repeat the process and build the parts in a layer-by-layer fashion.

For industry to adopt LPBF processes for production, robust quality assurance must be established [3]. In recent literature, the framework of in-process monitoring and control is highlighted as a potential approach to address quality issues. Grasso and Colosimo emphasized the two crucial needs of automated defect detection and process control strategies for developing smart LPBF systems [4]. Everton et al. remarked there is industry demand for in-situ inspection and closed-loop control techniques for AM. They proposed that a priori knowledge of the part and build process is necessary for closed-loop control [5]. Mani et al. demonstrated the need for real-time control of powder bed fusion processes by understanding the correlations between process parameters, process signatures and product qualities [6].

Given the significance of in-process monitoring to improve LPBF processes, the causes of common defects observed in LPBF processes have been reviewed. Malekipour and El-Monayri summarized typical defects existing in the LPBF process into four major categories, which are related to geometry and dimensions, surface quality, microstructure, and poor mechanical properties [7]. Grasso and Colosimo found six categories of defects, including geometric defects and surface defects, with four specified sources of defects for equipment, process, design for additive choices, and powder [4]. Similarly, Everton et al. listed five major LPBF discontinuities which are porosity within the material, as well as between layers, balling, unfused powder, and cracking [5].

A significant challenge of in-process monitoring associated with the LPBF processes is the difficulty to characterize part integrity using conventional methods, such as with a coordinate measuring machine (CMM), because LPBF processes typically take place within a closed chamber with limited space, and contact measurements could interfere with the process. Fringe projection, a non-contact and three dimensional (3D) measurement technique, has been proposed for surface metrology of metal AM parts [2] [8] as well as being implemented as an in-situ powder bed measurement technique [9]. However, there is limited reporting of deploying fringe projection as part of an in-process monitoring system. Zhang et al. proposed the implementation of fringe projection to measure the surface topography of a metal powder bed and showed that height maps contain information about the fusion process [9]. In addition to capturing the 3D surface of the powder bed area, Li et al. demonstrated that polymer powder beds are amenable to fringe projection system as contours of consolidated areas can be calculated for in-process control algorithms [10].

Unlike many 3D measurement techniques that only use cameras, fringe projection produces quantified measurements of the entire powder bed with minimal pixel correspondence issues. The data captured contain a representation of the surface in the form of a 3D point cloud. The information collected is helpful to derive insights about consolidation defects and dimensional inaccuracy. However, there is no perfect sensing system which can capture all types of defects. Hence, the fringe projection technique has its limitations, and one of these is the time taken to capture a large set of data points, which

might be longer than the typical layer build time. A typical scan of the fringe projection technique can take approximately 10 s, while the time between the beginning of one layer and the beginning of the next layer in the studied system is at least 10 s and becomes longer with larger and more complex parts. The time taken for the analysis of point clouds is needed to keep within the layer build time for understanding the current layer condition before proceeding to the next layer. However, this limitation can be solved by downsampling the required points needed for timely analysis of point clouds. Apart from the disadvantage of high acquisition time, fringe projection only measures the surface of the powder bed which has little to no information of the layers underneath [11].

Another current limitation of fringe projection as an in-process monitoring system is its need for calibration, which is required to map the measured points into real-world coordinates [12]. As well as a potentially challenging system calibration, availability of point cloud analysis techniques explicitly applied to the application of in-process monitoring is lacking. Additionally, the data structures and processing methods of 3D point cloud data are different from those applied to 2D imaging systems [13]. In a recent study, Southon et al. measured maximum height deviation from the powder bed measurement point clouds to demonstrate the capability of the fringe projection system to detect defects early, such as random defects and curling [14]. Southon et al. highlighted the potential of utilizing point clouds for process signature extraction as part of in-process monitoring and control system.

This work aims to demonstrate that curvature-based analysis of point clouds can produce useful features for detecting defects related to geometry and surface quality.

2. Methods

The term point cloud is defined as a set of points represented in a coordinate space. Rusu and Cousins explained the term as a data structure which represents a collection of multidimensional points [15]. Weinmann further defined the term as a collection of 3D points, which are characterized by spatial coordinates which may be assigned with additional attributes, such as intensity, color, thermal, and other information [16]. The point clouds in this study are acquired by a fringe projection system that projects structured light onto the part's surface and records the distortions of the light pattern induced by the part's geometry (the system is further detailed in [11]). The distorted patterns are captured by a camera and used in the reconstruction of the surface geometry using the least-squares phase shifting algorithm [17].

The topic of curvature estimation of 3D surfaces represented as point clouds can be found in literature as early as Kreyszig in 1959, who discussed a detailed overview of concepts related to the differential geometry of 3D surfaces [18]. Local primitives, such as surface normals, curvature, and the change of curvature may provide useful information for the understanding of scanned parts in the form of a point cloud. Both Porteous [19] and Giblin [20] studied the use of curvature information for analyzing and studying surface shape. Douros and Buxton presented a review on the curvature estimation topic and proposed a new surface curvature estimation using a quadric surface representation [21].

Bae and Lichti proposed using the change of curvature and approximate normal vector of the surface to determine the registration of point clouds [22]. Jovančević et al. presented a defect detection and characterization system based on local normal and curvature properties of point clouds for airplane exteriors [23]. Madrigal et al. proposed a model-based 3D descriptor based on surface normals of point clouds for automatic surface inspection [12]. Both articles approach the processed point clouds as 2D images which can be used for defect detection and surface inspection. Furthermore, Bartkowiak et al. studied the use of multi-scale areal curvature analysis on the surfaces fabricated by fused deposition modeling (FDM), one of seven types of AM processes identified by ISO/ASTM52900-15 [24].

The first feature used for the segmentation of point clouds in this paper is curvature information. Curvature characterizes a point by its principal curvatures ($\boldsymbol{\kappa}_1$, $\boldsymbol{\kappa}_2$), where $\boldsymbol{\kappa}_1$ and $\boldsymbol{\kappa}_2$are the maximum and the minimum curvatures of the surface at a point [25]. Gaussian curvature K is defined as $\boldsymbol{\kappa}_1\boldsymbol{\kappa}_2$, while mean curvature H is defined as $\frac{\boldsymbol{\kappa}_1 + \boldsymbol{\kappa}_2}{2}$. For estimating the curvature of a surface in 3D space, the quadratic approximation of a surface S [18] is used in the neighborhood of a point $P(x_0, y_0), f(x_0, y_0)$, assuming f is twice differentiated at (x_0, y_0). The equations for the Gaussian curvature and the mean curvature of S at P are defined as follows [26]

$$K = \boldsymbol{\kappa}_1\boldsymbol{\kappa}_2 = \frac{f_{xx}\, f_{yy} - f^2{}_{xy}}{(1+f^2{}_x+f^2{}_y)^2}, \quad (1)$$

$$H = \frac{\boldsymbol{\kappa}_1 + \boldsymbol{\kappa}_2}{2} = \frac{(1+f^2{}_x)f_{yy} - 2f_x\, f_y f_{xy} + (1+f^2{}_y)f_{xx}}{2(1+f^2{}_x+f^2{}_y)^{\frac{3}{2}}}. \quad (2)$$

Where f and its subscripts are used to indicate the first and second order local derivatives in x and $\boldsymbol{y}$. The second feature used in this work is prominence variation. This is calculated as the distance between each point and a locally fitted, least-squares mean plane [27], given by all neighboring points within a sphere of kernel radius.

The algorithm flow to calculate curvature and prominence variation is as follows: for each point P in the point cloud, a neighborhood of points, within the kernel radius, is selected. The kernel radius is defined as the radius of a sphere within a neighborhood of points for the curvature estimation and prominence variation calculation. With the points selected within the kernel radius, the fitted quadratic surface is computed and, therefore, the curvature values for the central point are calculated. For the prominence variation calculation, a fitted plane based on the least-squares method is computed for each point using the neighbors within a chosen kernel radius. The prominence variation values of each point are calculated based on the distance between each point and this plane. Last, the curvature values and prominence variation values are assigned back to the point P as additional information.

3. Experimental Study

3.1 Fringe projection data acquisition system

The fringe projection system used was a commercial white light scanner, NUB3D SIDIO XR. The nominal measurement pitch was 75 μm in all three orthogonal directions, with a build chamber volume of 200 mm × 150 mm × 90 mm, and a stated volumetric accuracy after calibration of 15 μm. The fringe projection system acquired the measurements through the operator observation window of a EOS P100 polymer powder bed fusion machine. For the in-process measurements of the powder bed surface, the viewing angle was roughly 55° from horizontal. The builds consisted of single tensile test specimens, with best measurement results being when the test specimens were closer to the front of the build chamber, due to reduced data drop out in the sections furthest from the fringe projection system. The build of a single tensile test specimen took thirty layers to finish and then the 3D scanning process continued for at least ten layers.

3.2 Point cloud curvature analysis flow

The point cloud measurements captured the powder consolidation due to sintering after each laser beam passed and the curvature values and prominence variation values of the point cloud were processed. Next, the point cloud measurements with the added information of curvature and prominence variation were converted into 2D images using the scattered interpolant method [28]. The 2D images showed the curvature maps and prominence variation map of both part and powder bed. At this stage, the curvature maps and the prominence variation map may highlight defects that deviate in term of shape, dimension or any unwanted surface geometry. The curvature maps were further processed for mask creation. The region of interest was specified as only the parts for the reduction of point clouds. The cropped regions from curvature maps and prominence variation map were then binarized based on Otsu's thresholding [29], to obtain the part outline. A final mask representing the outline of a part was obtained by dilation and erosion.

The purpose of the mask obtained in the previous step is to segment the parts from the powder bed area for defect analysis. A successful segmentation enables the analysis of any geometric defects occurring either in the parts or powder bed during each layer. The mask resulting from segmentation was applied to the height map to calculate average drop due to consolidation for the part. Furthermore, a different mask can be produced for each layer. From this, the mask of each layer was subtracted from the mask of the previous layer to detect the outline change over layers. In addition, a separate analysis of powder bed and the part can be undertaken for defect detection and defect characterization.

4. Results and Discussion

4.1 Curvature maps and prominence variation map

The curvature-based analysis methods are implemented for the acquired powder bed point clouds. Each 3D scanned layer of the single tensile strength specimens contains approximately 290 000 points. Both the curvature maps and the prominence variation map, which reveal catastrophic defects, warping, and geometric defects, are presented below.

4.1.1 Catastrophic defects

Figure 1 shows three surface analysis maps of the sintered layer of a part with observed debris on the right-hand side. The debris is a defect which could affect the part negatively. The debris is detected on the 16th layer of the print, where the right-hand side of the part is likely disrupted by the powder spreading blade. The unwanted debris is identified in all three surface analysis maps.

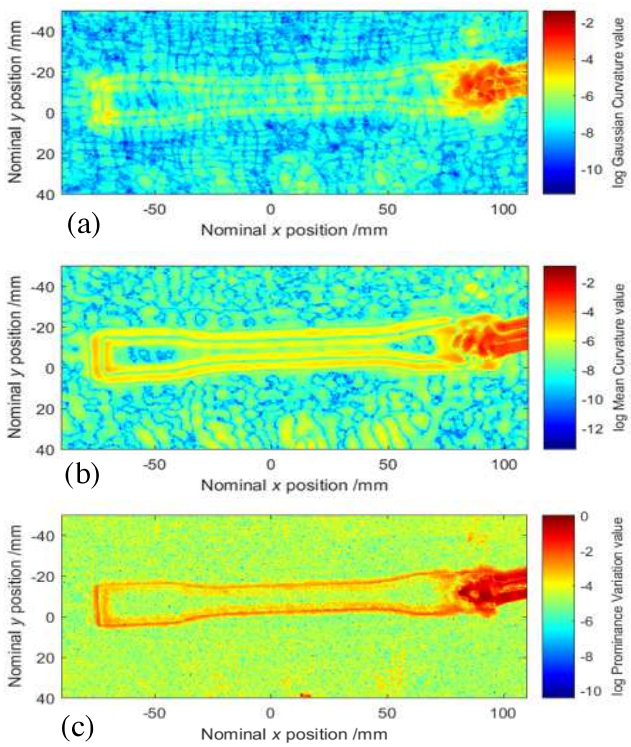

Figure 1. (a) Gaussian curvature map, (b) mean curvature map, c) prominence variation map of the 16th layer of a failed build with debris discovered on the right-hand side of the part. This tensile test piece was printed at 165 °C, 17 W laser power with a laser scan speed of 2500 mm/s and a hatch spacing of 250 μm.

4.1.2 Warping

Figure 2 (a), (b) and (c) show three surface analysis maps of the final sintered layer of a part, built with a laser power of 4 W, with severe warping on both ends. For the studied part, warping, another form of defect which is common in the LPBF process [30], is observed on many layers including the 30th layer of the specimen, see figure 2. Furthermore, heaping of surrounding powder can also be identified at about -30 mm in the x-direction. This phenomenon is similar to the observation made by Southon et al. in [14]. In an ideal LPBF process, the part should lay flat on the powder bed after laser sintering. However, the curling effect causes both ends of the part to be elevated. Therefore, the curvature of the warping issue is easily identified in all three surface analysis maps.

Even after the part has finished printing, the severity of warping can still be observed throughout the subsequent layers. Figure 2 (d), (e) and (f) show that the continuing effect of the curled ends of the part remains even after ten layers of new powder have been spread on top of the part. The elevated edges of the parts are observed in all three analysis maps while the center portion of the part is buried underneath the powder. This observation suggests that curvature-based analysis is effective at identifying features related to the issue of warping.

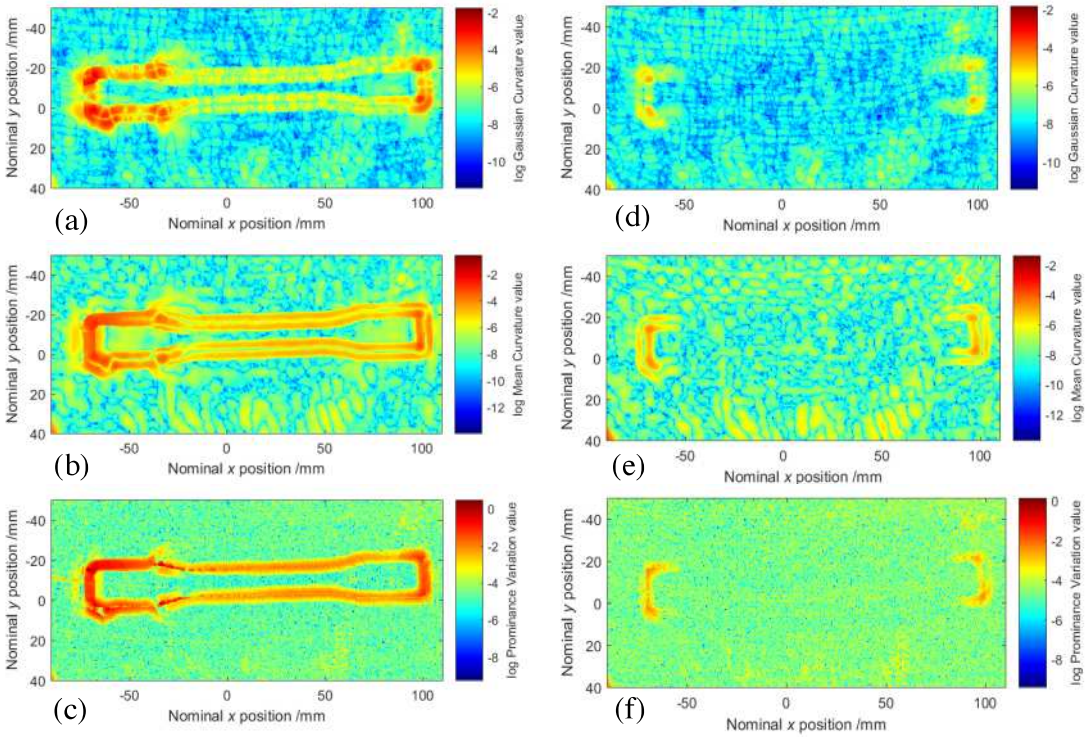

Figure 2. (a) Gaussian curvature map, (b) mean curvature map, (c) prominence variation map of the final sintered layer (30th layer) of a successful build with warping on both ends of the part. (d) Gaussian curvature map, (e) mean curvature map, (f) prominence variation map of the 40th layer of a build with the continuing effect of warping on both ends of the part.

4.1.3 Geometric defects in the part

Figure 3 (a), (b) and (c) show three surface analysis maps of the sintered layer of a part with a surface protrusion on the left edge of the top part at the 19th and 28th layers. The surface protrusion, which appears to be a geometric defect, is observed to begin on the 19th layer of the print and continually developed into a larger protrusion over subsequent layers. The prominence variation map seems to be less sensitive to surface defects, where only a smaller region of dots indicates the variation on the local surface. It should also be noted that a laser scanning line artifact, shown in Figure 3 (c) and (f), is captured on the prominence variation map. This laser scanning line artifact is likely to be a combination of individual laser scan lines because about 68 lines can be seen across the 165.2 mm length of the part, leading to a spacing of 2429.4 μm which is significantly larger than the 250 μm scan spacing of the laser path.

In the parts measured which were printed at 165 °C with higher laser power, 27 W and the same scan speed of 2500 mm/s, a random defect occurred on at the 19th layer. The observation suggests that a geometric defect, such as a surface protrusion, could occur randomly even with process parameters close to optimal. Hence, the fringe projection can satisfy the need for in-process monitoring to detect random defects.

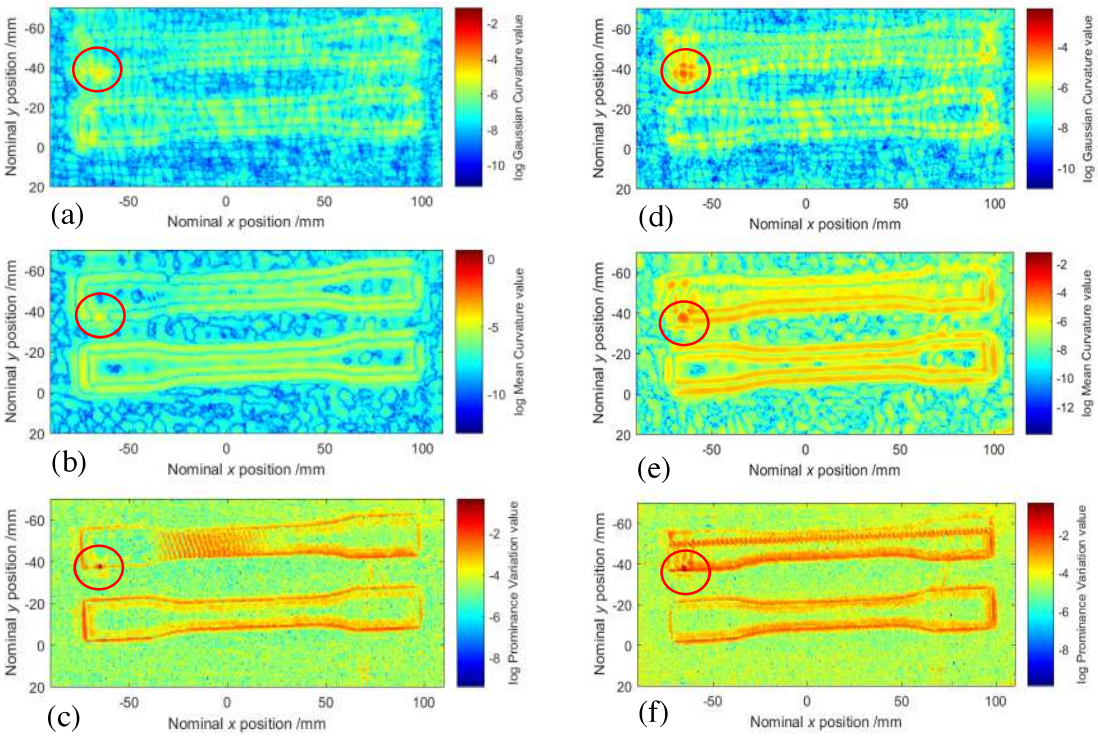

Figure 3. (a) Gaussian curvature map, (b) mean curvature map, (c) prominence variation map of the 19th layer where a surface protrusion, as marked with a red circle, on the left side of the top part. (d) Gaussian curvature map, (e) mean curvature map, (f) prominence variation map of the 28th layer where the observed surface protrusion is larger and in the same region of the top part.

4.2 Curvature based segmentation for mask creation

The curvature and prominence variation maps are useful for defect identification on each acquired layer point cloud. However, the need to perform segmentation of parts from the powder bed is critical in differentiating the location of defects occurring in each layer. Therefore, the successful segmentation is essential to recognize the severity of defects by their location. The following results present the curvature-based segmentation with a mask created using Gaussian curvature, mean curvature and prominence variation, which captures the shape of the part. Figure 4 (a), (b) and (c) show the results of the three initial masks after binarizing the respective maps based on Otsu's thresholding.

In figure 4 (a), the mean curvature-based mask is successful at detecting the edges of the parts; the black region between two white regions indicates the edge of the part, while white regions indicate areas surrounding the edge. In figure 4 (b), the Gaussian curvature-based mask consists of several blobs surrounding the edge of the part, and the blobs are useful for corner detection, where the corner of the mean curvature-based mask is missing. In figure 4 (c), the prominence variation-based mask performs better than the other two masks at outlining the edge of part despite noisy points.

In summary, each initial mask provides additional cues, and they complement each other when creating the final mask. With the combination of the three initial masks, the final mask can capture the complete shape of a part, which is shown in figure 4 (d) and (e).

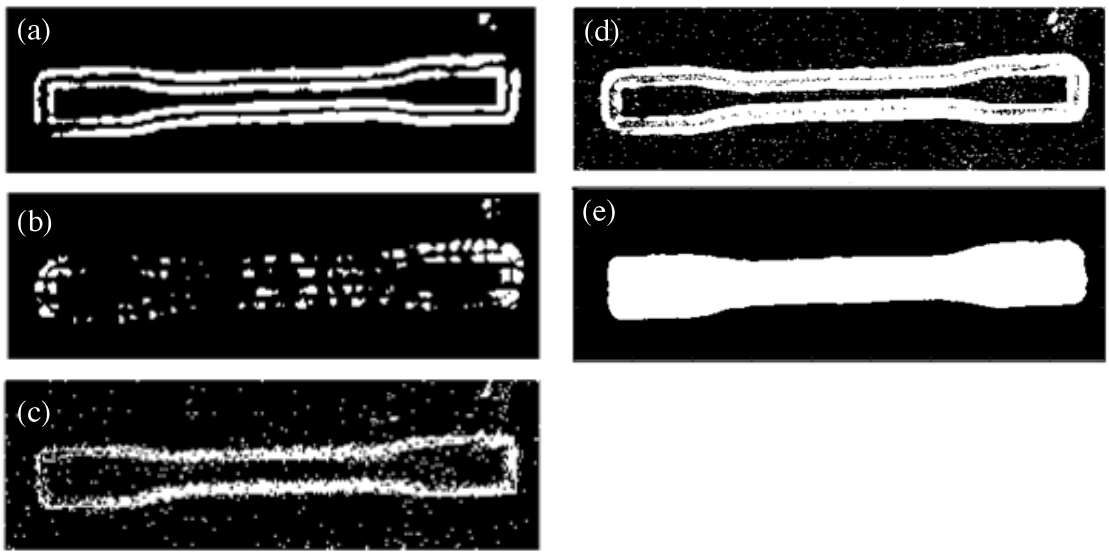

Figure 4. (a) mean curvature mask (b) Gaussian curvature mask (c) prominence variation mask after binarizing surface analysis maps based on Otsu's thresholding. (d) the result of a combination of three initial masks which represent the shape of part (e) the final mask is created after implementing the image processing methods of erosion and dilation.

4.2.1 Computation of drop due to consolidation

By applying the curvature-based mask to segment the part from the powder bed, the analysis of powder bed point clouds for an in-process monitoring system can be improved. One of the process signatures for in-process monitoring is drop due to consolidation, which provides a basic understanding of the quality of consolidation of layers [9]. Figure 5 and figure 6 show the segmentation mask applied to the height map and the computation of the average drop due to consolidation in each layer for point clouds taken at a laser power of 17 W. As Zhang et al. discussed, the average height drop is expected to converge to a constant value after an initial decrease in the first few layers [1].

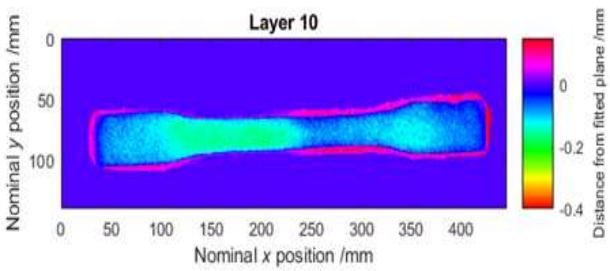

Figure 5. Example of a successful segmentation masking applied to a powder bed height map to compute the average drop due to consolidation. However, there is a small portion of the powder bed captured within the mask. The information of powder bed surrounding the part might be accounted into the computation of the average drop which leads to A slight inaccuracy of the computation. However, this issue can be solved by filtering out the positive values which appear to be part of the powder bed region.

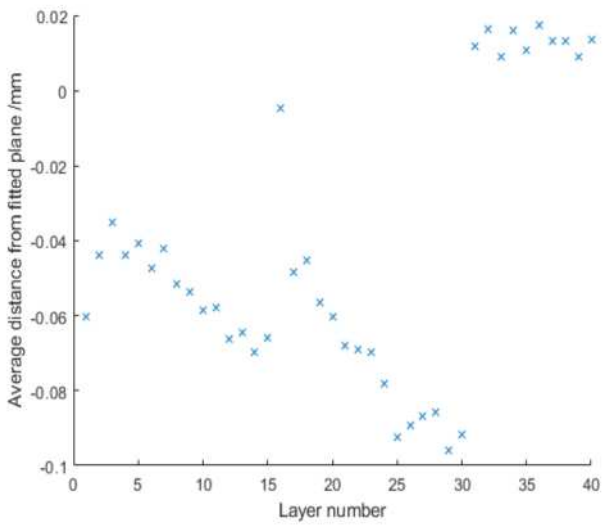

Figure 6. Average drop due to consolidation for the test part printed at 165 °C with a laser power of 17 W and a scan speed of 2500 mm/s. Drop due to consolidation increases with increasing layer count before layer 16 where the debris, shown previously, occurs. From the 16th layer to the 30th layer, the average drop due to consolidation showed a similar trend. From the 31st layer to the 40th layer, the positive values of drop indicate that the part is done and a new layer of powder is deposited, without laser sintering, on each layer.

4.2.2 Binarized outline change over layers

The powder bed of each layer can be separated into part and powder bed using the segmented mask. By subtracting each layer's segmentation mask from the previous layer mask, a three-valued map, showing the shifts of the contour defining the boundary of the parts, is created. The two signed values (-1, +1) indicate as the change of the previous layer and the current layer while 0 value indicates no change between layers. This technique can help identify powder heaping, which is likely caused by ineffective bed-spreader contact dynamics [31]. Figure 7 shows the detection of alternating heaping of powder from the 13th layer to the 15th layer as well as the detection of the deviation of part mask outlines between layers.

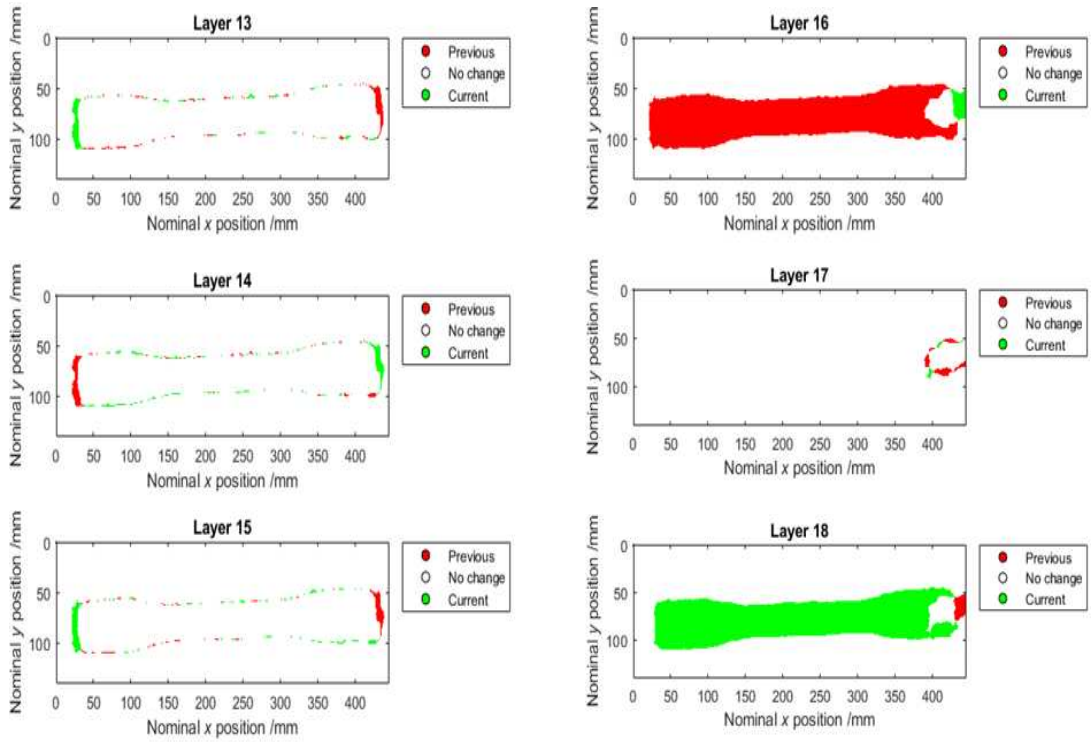

Figure 7. From the 13th layer to the 15th layer, fringe projection point clouds capture the alternate pattern of heaping of powder. The EOS P100 uses a straight metal powder spreading blade that travels in an arc across the powder bed. The accumulated powder at the alternating ends suggests that the powder spreading blade might not wholly smooth the powder over the submerged, consolidated part. From the 16th layer to the 18th layer, a series of layer changes is shown with a noticeable deviation from the outline shape of the part.

4.2.3 Separate analysis of powder bed and part

Another contribution of the segmentation mask is to enable separate analysis of the powder bed and part. Separate analysis of powder bed and part is significant in improving the defect classification. Figure 8 (a) and (b) show the powder bed and the part at layer 16, where the debris is detected within the part and also in the powder bed. Figure 8 (c) and (d)

show the curling effect is observed on the powder bed and the part on the 31st layer. The ability to split out the part and the powder bed is critical because the separate analysis can show the location of defects. By knowing the location of defects, the severity of the defects can be determined and can inform the system whether to continue or stop the printing process.

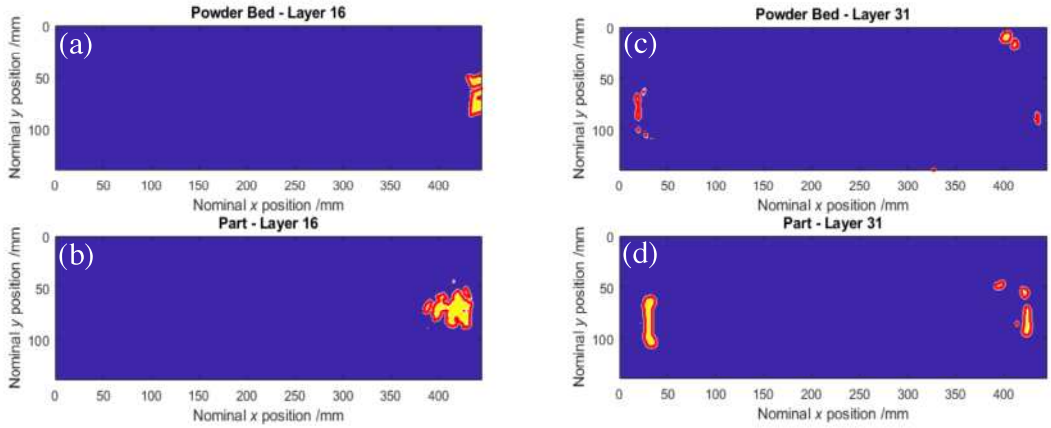

Figure 8. (a), (b) Separate analysis of the powder bed and the part where debris is observed on the 16th layer. (c), (d) Separate analysis of powder bed and the part where warping is observed on the 31st layer.

Conclusion

In summary, this work demonstrates that the curvature analysis of point clouds acquired by a fringe projection system can be used for in-process monitoring of powder bed fusion to identify catastrophic defects, warping, and geometric defects. Furthermore, the curvature and prominence variation information can be used to create segmentation masks for the powder bed and part. This study has demonstrated that a segmentation mask with no a priori part information can be created and can be used to compute drop due to consolidation in the region of interest. Also, the segmentation masks enable detection of changes in the outline of the consolidated areas between layers by comparing the outline of successive layers. The alternate pattern of heaping of powder and outline shape deviation of a layer can also be observed. Another contribution of curvature-based segmentation is the separate analysis of the powder bed and the part which allows for localization of defects.

The insights extracted from the point clouds analysis can be used to inform process control strategies. The drop due to consolidation is a significant process signature for determining the quality of layer processing [14]. Being able to compute the average drop from the height map with an automatic segmentation mask, provides information that can be used to further the understanding of polymer LPBF. Also, the binarized outline change over layers could be utilized as an alert for early defect detection during a build. The mask analysis of the outline change of each layer can be studied for feature extraction suitable for machine learning classification applications. The output of the separate analysis of both powder bed and the part can further identify defect types and defect characterization. With

a priori knowledge of the potential causes of each defect type, an in-process closed-loop feedback system could be implemented for tuning the optimal values of LPBF process parameters.

The aim of the next implementation of this research is using curvature-based segmentation of LPBF point clouds as a real-time analysis tool for in-process defect detection and classification. A new study on defect classification and associated causes is ongoing. In conclusion, the application of the novel framework developed herein using a fringe projection system for in-process monitoring and analysis in a powder bed fusion AM process will be performed on a real case study.

Acknowledgments

This work was supported by the Engineering and Physical Sciences Research Council [grant number EP/M008983/1, EP/L01534X/1]

References

[1] W.S. Land, B. Zhang, J. Ziegert, A. Davies, In-situ metrology system for laser powder bed fusion additive process, Procedia Manuf. 1 (2015) 393–403. doi:10.1016/j.promfg.2015.09.047.

[2] Dickins, T. Widjanarko, S. Lawes, P. Stravroulakis, R. Leach, Design of a multi-sensor in-situ inspection system for additive manufacturing, Proc. ASPE/euspen Advancing Precision in Additive Manufacturing. (2018) 248-242.

[3] S.A.M. Tofail, E.P. Koumoulos, A. Bandyopadhyay, S. Bose, L. O'Donoghue, C. Charitidis, Additive manufacturing: scientific and technological challenges, market uptake and opportunities, Mater. Today. 21 (2018) 22–37. doi:10.1016/j.mattod.2017.07.001.

[4] M. Grasso, B.M. Colosimo, Process defects and in situ monitoring methods in metal powder bed fusion: A review, Meas. Sci. Technol. 28 (2017). doi:10.1088/1361-6501/aa5c4f.

[5] S.K. Everton, M. Hirsch, P. Stravroulakis, R.K. Leach, A.T. Clare, Review of in-situ process monitoring and in-situ metrology for metal additive manufacturing, Mater. Des. 95 (2016) 431–445. doi:10.1016/j.matdes.2016.01.099.

[6] M. Mani, B. Lane, A. Donmez, S.S.C.S. Feng, S.S.P. Moylan, R. Fesperman, M.A. Donmez, S.S.C.S. Feng, S.S.P. Moylan, R. Fesperman, Measurement science needs for real-time control of additive manufacturing powder bed fusion processes, (2015) 50. doi:10.6028/NIST.IR.8036.

[7] E. Malekipour, H. El-Mounayri, Common defects and contributing parameters in powder bed fusion AM process and their classification for online monitoring and control: a review, Int. J. Adv. Manuf. Technol. 95 (2018) 527–550. doi:10.1007/s00170-017-1172-6.

[8] P.I. Stavroulakis, R.K. Leach, Invited Review Article: Review of post-process optical form metrology for industrial-grade metal additive manufactured parts, Rev. Sci. Instrum. 87 (2016). doi:10.1063/1.4944983.

[9] B. Zhang, J. Ziegert, F. Farahi, A. Davies, In situ surface topography of laser powder bed fusion using fringe projection, Addit. Manuf. 12 (2016) 100–107. doi:10.1016/j.addma.2016.08.001.
[10] Z. Li, X. Liu, S. Wen, P. He, K. Zhong, Q. Wei, In-situ 3D monitoring of geometric signatures in powder-bed-fusion additive manufacturing process via vision sensing methods, (2018) 1–14. doi:10.3390/s18041180.
[11] S. Van der Jeught, J.J.J. Dirckx, Real-time structured light profilometry: a review, Opt. Lasers Eng. 87 (2015) 18–31. doi:10.1016/j.optlaseng.2016.01.011.
[12] C. Madrigal, J. Branch, A. Restrepo, D. Mery, A method for automatic surface inspection using a model-based 3D descriptor, Sensors. 17 (2017) 2262. doi:10.3390/s17102262.
[13] M. Weinmann, Introduction, in: Reconstr. Anal. 3D Scenes From Irregularly Distrib. 3D Points to Object Classes, Springer International Publishing, Cham, 2016: pp. 1–15. doi:10.1007/978-3-319-29246-5_1.
[14] N. Southon, P. Stavroulakis, R. Goodridge, R. Leach, In-process measurement and monitoring of a polymer laser sintering powder bed with fringe projection, Mater. Des. 157 (2018) 227–234. doi:10.1016/j.matdes.2018.07.053.
[15] R.B. Rusu, S. Cousins, 3D is here: point cloud library, IEEE Int. Conf. Robot. Autom. (2011) 1–4. doi:10.1109/ICRA.2011.5980567.
[16] M. Weinmann, Preliminaries of 3D point cloud processing, in: Reconstr. Anal. 3D Scenes From Irregularly Distrib. 3D Points to Object Classes, Springer International Publishing, Cham, 2016: pp. 17–38. doi:10.1007/978-3-319-29246-5_2.
[17] K. Creath, Phase-measurement interferometry techniques, Prog. Opt. 26 (1988) 349–393.
[18] E. Kreyszig, Introduction to differential geometry and Riemannian geometry, University of Toronto Press, 1968.
[19] I.R. Porteous, Geometric differentiation, (1994).
[20] J.W. Bruce, P.J. Giblin, F. Tari, Ridges, crests and sub-parabolic lines of evolving surfaces, Int. J. Comput. Vis. 18 (1996) 195–210.
[21] I. Douros, B.F. Buxton, Three-dimensional surface curvature estimation using quadric surface patches, Scanning. 44 (2002).
[22] K.-H. Bae, D.D. Lichti, A method for automated registration of unorganised point clouds, ISPRS J. Photogramm. Remote Sens. 63 (2008) 36–54.
[23] I. Jovančević, H.-H. Pham, J.-J. Orteu, R. Gilblas, J. Harvent, X. Maurice, L. Brèthes, 3D Point cloud analysis for detection and characterization of defects on airplane exterior surface, J. Nondestruct. Eval. 36 (2017) 74. doi:10.1007/s10921-017-0453-1.
[24] ASTM ISO/ASTM52900-15 Standard terminology for additive manufacturing – general principles – terminology, (2015).
[25] J. Jiang, J. Cheng, X. Chen, Registration for 3-D point cloud using angular-invariant feature, Neurocomputing. 72 (2009) 3839–3844.
[26] Z. Har'el, Curvature of curves and surfaces–a parabolic approach, Dep. Math. Tech. Inst. Technol. (1995).
[27] V. Schomaker, J. Waser, R.E. Marsh, G. Bergman, To fit a plane or a line to a set of points by least squares, Acta Crystallogr. 12 (1959). doi:10.1107/S0365110X59001748.

[28] I. Amidror, Scattered data interpolation methods for electronic imaging systems: a survey, J. Electron. Imaging. 11 (2002) 157. doi:10.1117/1.1455013.
[29] N. Otsu, A threshold selection method from gray-level histograms, IEEE Trans. Syst. Man. Cybern. 9 (1979) 62–66.
[30] R.D. Goodridge, C.J. Tuck, R.J.M. Hague, Laser sintering of polyamides and other polymers, Prog. Mater. Sci. 57 (2012) 229–267. doi:10.1016/j.pmatsci.2011.04.001.
[31] S. Haeri, Y. Wang, O. Ghita, J. Sun, Discrete element simulation and experimental study of powder spreading process in additive manufacturing, Powder Technol. 306 (2017) 45–54. doi:10.1016/j.powtec.2016.11.002.